10 November 1995

ELSEVIER

Chemical Physics Letters 245 (1995) 605–614

CHEMICAL PHYSICS LETTERS

Angle–velocity-resolved measurements of $I(^2P_{3/2,1/2})$ from $(CH_3I)_n$ cluster photodissociation at 266 and 304 nm

Jack A. Syage

The Aerospace Corporation, P.O. Box 92957, M5-754, Los Angeles, CA 90009, USA

Received 11 July 1995; in final form 29 August 1995

Abstract

The angle–velocity distribution of $I(^2P_{3/2})$ and $I(^2P_{1/2})$ from photodissociation of $(CH_3I)_n$ clusters was measured at 266 and 304 nm. For the monomer ($n = 1$), the angular distribution is very anisotropic and the translational energy spectrum is sharply peaked at high energy. For clusters (predominantly $n = 2$, 3), the I atom undergoes collisions, which substantially relax the translational energy and anisotropy. Three observations are reported. (1) A residual anisotropy exists in cluster photodissociation that increases with increasing fragment translational energy. (2) The I atom $^2P_{3/2}$ to $^2P_{1/2}$ branching ratio increases significantly in clusters relative to monomer. (3) TOF spectra were observed for I atoms originating from photodissociation of the cluster photoproduct I_2. These observations are discussed in terms of a caging of I atoms that may either react or escape from the cluster.

1. Introduction

Studies of photofragmentation in isolated molecules provide detailed understanding of reaction dynamics and descriptions of potential energy surfaces. In this work we report state-specific and angle–velocity resolved measurements of reaction products from the photodissociation of molecular clusters. In isolated molecules, this level of detail in probing photofragments is usually sufficient to determine the potential energy surface traversed by the half-collision dissociation, provided the initial geometry is known. Our interest in applying detailed probes of photofragments from cluster excitation is to learn about multiple collision interactions of the type normally associated with condensed-phase phenomena, such as translational, vibrational, and rotational relaxation. If we assume that clusters are an analog to condensed-phase behavior, than unprecedented detail on collisional energy relaxation in the bulk can be obtained.

Spectroscopic studies of reaction products from van der Waals molecules were introduced by Soep and co-workers [1,2] and Wittig and co-workers [3–5] (we distinguish this chemistry from the more extensive studies of van der Waals dissociation). The former group studied a series of excited state dimer reactions of the type $HgX_2^* \rightarrow HgX^* + X$ ($X = Cl_2$, H_2) and measured product rovibrational distributions from dispersed fluorescence spectra of electronically excited HgX^*. Wittig's group measured OH and CO product internal energy distributions for CO_2–HX complexes (X = Cl, Br and I) by laser induced fluorescence [3,4]. These complexes assume specific equilibrium geometries, that vary with X, providing the means to explore chemical dynamics for pre-

SSDI 0009-2614(95)01051-3

aligned collision parameters. The complex reaction $H + CO_2$ forms $OH + CO$ with a reaction efficiency and partitioning of energy into rotation and vibration that depends strongly on the bimolecular alignment. Femtosecond domain experiments have been developed by the groups of Zewail [6,7] and Wittig [5] for the same systems. The Zewail group has also introduced femtosecond kinetic energy time-of-flight spectroscopy for measuring time-dependent fragment velocity distributions [8].

The measure of product translational energy from photoinitiated cluster reactions is emerging as a powerful tool. Many studies have focused on cluster ion photodissociations [9–11]. In these studies, ion fragments are convenient to detect; however, internal state distributions are not typically measured. For neutral dissociation, the fragments must be probed, which is usually done in a state-specific manner by resonance ionization or fluorescence detection. In studies of neutral CH_3I monomer photodissociation, Ogorzalek Loo et al. [12] and Penn et al. [13] observed that cluster formation broadens the time-of-flight spectrum for I atom. The monomer dissociation is known to be very anisotropic with a velocity distribution sharply peaked at high energy. The product velocity distribution for the clusters, however, was broad and peaked at zero component-velocity. Wittig has recently implemented a method for measuring the translational energy distribution for H atoms scattering out of photoinitiated complexes such as Ar–HX (X = Br, I) [14]. By exciting dissociated H atom to high n Rydberg states and field ionizing them at the detector, they have achieved very high velocity resolution (by avoiding space charge repulsion). The Miller group has applied the novel use of a strong electric field to orient complexes such as N_2–HF for measuring angle–resolved properties in the molecular frame [15].

In the present study, we recorded the angular dependence of the I atom velocity distribution in the $^2P_{3/2}$ and $^2P_{1/2}$ state (henceforth I and I^*) following excitation of $(CH_3I)_n$ ($n = 1$–3) at 266 and 304 nm. As noted by Ogorzalek Loo et al. [12] and Penn et al. [13] above, the results are remarkably different from that recorded for photodissociation of the isolated molecule CH_3I. We have measured the angle-dependent translational energy distribution and product branching ratio I/I^*. Young has recently measured I atom and H atom translational energy spectra for $(HI)_n$ cluster photodissociation [16]. An interesting observation in their work is the detection of I atom originating from product I_2 photodissociation, in addition to I atom scattering from the cluster. We have observed similar signals for $(CH_3I)_n$, which we present in this work. The work by our group and by Young are probing cage escape dynamics of I atom and, therefore, complement measurements of cage recombination in clusters and bulk phase. Ultrafast spectroscopy has recently been applied to measure I_2 recombination in rare gas clusters by the Zewail group [17] and I_2^- recombination in CO_2 clusters by the Lineberger group [18]. Though the present work does not measure I_2 dissociation, the technique used here is potentially valuable to this problem because it probes the conditions for which caging does not occur. The dissociated I atom in $(CH_3I)_n$ photolysis is known to undergo intracluster chemistry leading to I_2 formation, so the escape of I atom competes with I_2 formation [19–22].

The Ziegler group [21] and the Donaldson group [22] measured the vibrational distribution of the I_2 product from $(CH_3I)_n$ photolysis. The former investigators measured a vibrational temperature of about 1000 K for 200 nm photolysis. The latter study at 193 and 248 nm photolysis, however, is consistent with a rovibrational distribution having an upper limit of 300 K. We will discuss these results in greater detail in Section 5.

2. Experimental

Details of our experimental apparatus for measuring angle–velocity distributions has been described before [23]. Our time-of-flight mass spectrometer consists of an ion optics assembly of three grids separated by 1 cm, a 1 m drift tube, and an aperture of radius $r = 5$ mm mounted in front of an 18 mm diameter microchannel plate detector. The results presented here were collected using 30 and 480 V/cm for the extraction and acceleration fields, respectively. Under these operating conditions, I^+ ions have flight times centered at $t_0 = 42$ μs. The fragment three-dimensional spatial distribution expands as it travels down the drift tube to the detector. The detection aperture limits the field-of-view to a

cylinder of ions of maximum radial velocity $v_r = r/t_0$. A combination of the detector aperture diameter and blurring of the ion image due to diffraction off grids currently limits our spatial resolution to about 8 mm, corresponding to a radial resolution of $v_r = 0.10$ km/s.

The angular and energy resolutions are dependent on photofragment speed v and are given by

$$\Delta\theta_z = \arcsin(v_r/v) \quad \text{(angular resolution)}, \tag{1}$$

$$\Delta v/v = 1 - v_{z,\min}/v = 1 - \cos\Delta\theta_z \quad \text{(energy resolution)}, \tag{2}$$

where $v_{z,\min} = (v^2 - v_r^2)^{1/2}$. The detection cylinder limits the range of v_z corresponding to a particular v, which defines Δv. As v_r decreases relative to v, the detected v_z distribution becomes a good measure of the speed distribution v. In the present work, we probe through the center of the ion 3D velocity distribution at different angles α. In previous work, we recorded series of 1D TOF spectra by sequentially offsetting the detection cylinder from the center line, thereby mapping out a 2D section of the 3D velocity distribution [23,24]. These concepts are developed mathematically in Section 3.

Photolysis was initiated at 266 nm or 304 nm. I and I^* photofragments were ionized by 2 + 1 resonance-enhanced multiphoton ionization (REMPI) using excitation at 304.7 nm ($^6P\,^2D^o_{5/2}$ intermediate state) and 304.0 nm ($^6P\,^4D^o_{1/2}$ state), respectively. For 266 nm photolysis, the pump pulse precedes the probe pulse by about 10 ns. For 304 nm photolysis, the pump and probe pulses are the same. The laser polarization angle α of the pump was varied by rotating a combination of a double Fresnel-Rhomb and a Glan-Taylor polarizer. Flat windows were used on the molecular beam port to minimize polarization-dependent transmission. The incident pump and probe laser pulse energies were measured using a photodiode at the exit window of the molecular beam. Laser pulse energies and focusing conditions were adjusted to avoid space charge repulsion and in the case of 266 nm photolysis to maximize the two-pulse signal relative to the one-color signal. TOF spectra were collected using a LeCroy 9450 digital scope.

The CH_3I sample was placed in a bubbler cooled to 0°C and delivered to the pulsed valve by a flow of Ar at 1000 Torr (results were unchanged at lower temperatures). To reduce cluster formation, the pulsed valve was heated to 60°C. Near cluster-free monomer TOF spectra could be obtained by synchronizing laser excitation to the leading edge of the gas pulse. Increasing amounts of cluster signal could be obtained by moving the laser excitation toward the peak of the gas pulse.

The present core sampling technique is similar to that developed by the groups of Houston [25], El-Sayed [26] and Chandler [27]. These investigators use delayed ion extraction to achieve large separation of the velocity components, but the non-space focusing conditions complicate the relationship between v_z and $t - t_0$. We have opted for space focusing conditions because of the linear relation between v_z and $t - t_0$ as discussed next.

3. Model for measuring differential cross sections

The differential cross section for photodissociation with respect to fragment speed v and recoil solid angle Ω is given by

$$\frac{d^2\sigma}{d\Omega\,dv} = \frac{d\sigma}{d\Omega}g(v) = \frac{\sigma}{4\pi}\left[1 + \beta P_2(\cos\theta)\right]g(v) = \frac{d\sigma}{d\Omega}g(v) = \frac{\sigma}{4\pi}\left[1 + \beta P_2(\cos\alpha)\,P_2(\cos\theta_z)\right]g(v). \tag{3}$$

The separation of the angular and velocity distributions is strictly valid for collisionless photodissociation, but less valid for cluster photodissociation where collisions affect the angle–velocity distributions. In the limit of multiple-collisions or long-lifetime cluster residence time leading to an isotropic distribution, $g(v)$ becomes independent of angle once again. In the second line of Eq. (3), we have transformed to the laboratory drift tube z axis where $d\Omega = \sin\theta_z\,d\theta_z\,d\varphi_z = 2\pi\sin\theta_z\,d\theta_z$ is the laboratory-frame solid angle. The angle θ is the recoil angle relative to the electric field axis ϵ and α is the angle of ϵ relative to the z axis. Hence the photofragment recoil angle relative to the z axis is $\theta_z = \theta + \alpha$. The

second Legendre polynomial is defined as $P_2(x) = (3x^2 - 1)/2$ and β is the anisotropy factor for the angular distribution. The maximum anisotropies for parallel and perpendicular transitions are 2 and -1, respectively, and a value of 0 corresponds to an isotropic angular distribution.

The flux of ions along the z axis per unit time and radial position is given by

$$\frac{d^2N}{dt\,dv_r} = \kappa\frac{d\sigma}{d\Omega}g(v)\left(\frac{d\Omega}{dv_z}\frac{dv_z}{dt}\frac{dv}{dv_r}\right)$$

$$= \kappa\frac{d\sigma}{d\Omega}g(v)\left(\frac{-2\pi}{v}\frac{qE}{m}\frac{v_r}{v}\right), \quad (4)$$

where the evaluation of $d\Omega/dv_z$ follows from solid-angle considerations [24] and dv_z/dt is obtained under space focusing where q is the ion charge, E is the ion drift energy, and m is ion mass. Under non-space focusing conditions, dv_z/dt is a complicated function. The κ term encompasses a set of constants that includes laser intensity, molecular beam density, ionization efficiency, and detection sensitivity.

The observed TOF spectrum $I(v_z)$ is obtained by integrating over the aperture size as follows:

$$I(v_z) = \int_0^{v_r}\frac{d^2N}{dt\,dv_r}dv_r' = \kappa\int_0^{v_r}\frac{d\sigma}{d\Omega}\frac{g(v)}{v^2}v_r'\,dv_r'. \quad (5)$$

We have evaluated Eq. (5) elsewhere for various examples of anisotropies, functional forms of $g(v)$, and aperture sizes ranging from core sampling to 1D projections [24]. Here we present an abbreviated account pertinent to the present results. For core sampling conditions, where $v_r < v$ and $g(v)$ is slowly varying over dv_r, Eq. (5) simplifies to

$$I_\alpha(v_z) = \kappa\frac{v_r^2}{v_z^2}\frac{d\sigma}{d\Omega_\alpha}g(v). \quad (6)$$

In this limit $v \approx v_z$, in which case the product $v_z^2 I_\alpha(v_z)$ directly measures the differential cross section for the fragment scattering angle $\theta = \alpha$. When $v_r \ll v$ is not satisfied, such as when v is small, v_z ceases to be a good measure of v. Then the integral in Eq. (5) must be carried out explicitly in order to fit a calculated $I(v_z)$ to observed measurements.

One method for fitting data is to take a trial $g(v)$

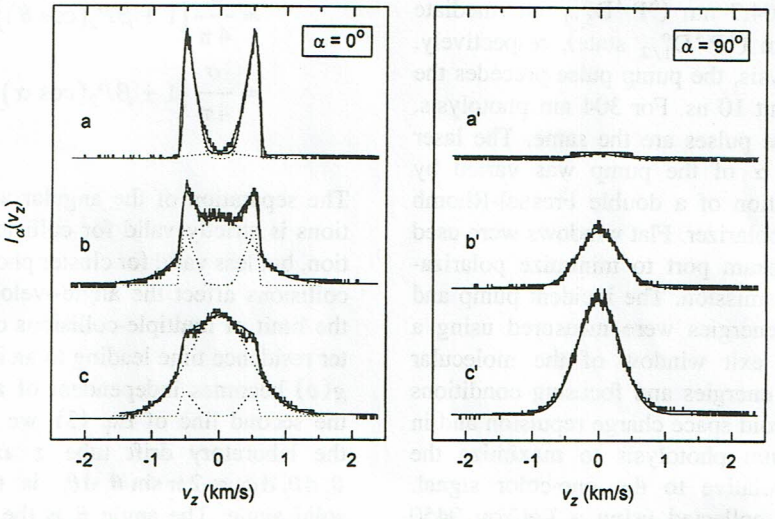

Fig. 1. Angle-resolved $I(^2P_{3/2})$ photofragment velocity distributions $I_\alpha(v_z)$ for $(CH_3I)_n$ excitation at 266 nm where α is the alignment of ϵ relative to the drift tube z axis and $\theta = \alpha$ is the product recoil angle relative to ϵ. (a, a′) monomer excitation, (b, b′) monomer and cluster excitation, (c, c′) increasing cluster distribution. Calculated fits are shown (———) along with the individual contributions due to monomer and cluster excitation (· · ·).

and calculate TOF distributions for individual increments of v and adding the results to obtain $I(v_z)$. This is done for the CH_3I monomer dissociation, which is very anisotropic ($\beta \approx 2$) and has a highly peaked speed distribution $g(v)$. An important simplification occurs when $\beta = 0$ and $g(v)$ can be described by a Maxwell–Boltzmann distributions (i.e. $g(v)\,dv = \exp(-v^2/\sigma_v^2)v^2\,dv$, where σ_v is the Gaussian width). Eq. (5) then becomes (after a change of variables $v_r\,dv_r = v\,dv$)

$$I(v_z) = \kappa \int_{v_{min}}^{v_{max}} \exp(-v^2/\sigma_v^2)\, v\,dv$$
$$= \tfrac{1}{2}\kappa\sigma_v^2 \exp(-v_z^2/\sigma_v^2) \times \left[1 - \exp(-v_r^2/\sigma_v^2)\right]. \quad (7)$$

The limits of integration define the range of values v that contribute to $I(v_z)$ at a particular value of v_z and are given by $v_{min} = v_z$ and $v_{max} = (v_z^2 + v_r^2)^{1/2}$. Eq. (7) describes the interesting property of isotropic Maxwell–Boltzmann distributions that any 1D cylindrical slice of the 3D Gaussian distribution gives the same shaped curve for $I(v_z)$. The relation $v_z^2 I(v_z) \propto g(v)$ is, therefore, equally valid for 1D projection and core sampling conditions.

The probability distribution for fragment translational energy is obtained from the relation $P(E)\,dE = g(v)\,dv$, which gives $P(E) = g(v)/mv$. Under core sampling conditions, Eq. (6) leads to

$$P(E_t) = \left(\frac{\kappa m v_r^2}{v_z}\frac{d\sigma}{d\Omega_\alpha}\right)^{-1} I_\alpha(v_z), \quad (8)$$

where $E_t = mv_z^2/2$ is the fragment kinetic energy. For an isotropic Maxwell–Boltzmann distribution, $P(E_t) \propto v_z I_\alpha(v_z)$ regardless of the radial resolution v_r. The c.m. translational energy is computed from

$$E_{t,c.m.} = E_t \frac{M}{M-m}, \quad (9)$$

where m is the detected fragment mass and M is the molecular precursor mass.

4. Results and analysis

Observed TOF traces $I_0(v_z)$ and $I_{90}(v_z)$ are presented in Fig. 1 for the detection of the $I(^2P_{3/2})$ photofragment from the 266 nm photolysis of $(CH_3I)_n$ monomers and clusters. The series of Figs. 1a,a′ to 1c,c′ represent conditions of increasing clustering. Calculated curves are fitted to the data in Fig. 1. The curve fits to the monomer results were calculated from Eq. (5) using the known $g(v)$ distribution recorded at higher resolution and the instrument function $n(v_r, v)$ corresponding to the present experiment. The curve fits to the cluster results were calculated from a single Gaussian function. The following observations are evident in Fig. 1.

(1) With increasing clustering, a broad peak centered at $v_z = 0$ emerges for photofragment recoil at 0 and 90° relative to ϵ.

(2) For cluster photodissociation, the width of the $I_{90}(v_z)$ distribution is narrower than for the $I_0(v_z)$ distribution.

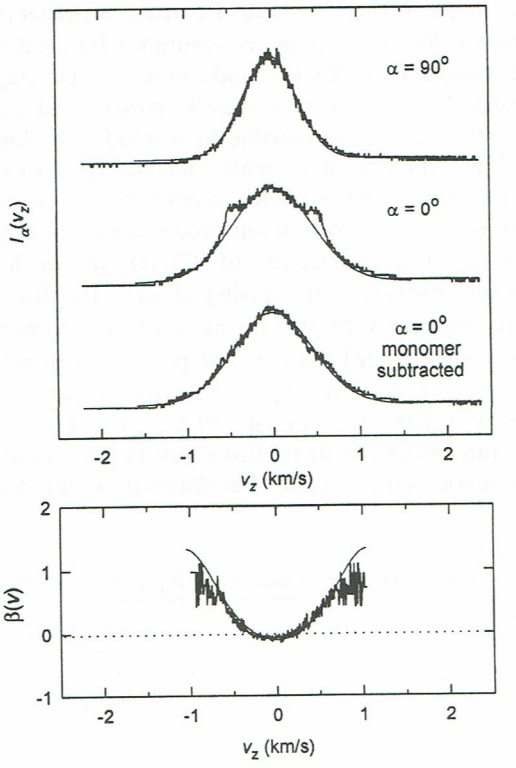

Fig. 2. Velocity spectra $I_\alpha(v_z)$ and velocity-dependent anisotropy $\beta(v)$ for $(CH_3I)_n$ cluster excitation at 266 nm and $I(^2P_{3/2})$ detection. The $I_\alpha(v_z)$ spectra were fitted to Gaussian functions (———) of the form $\exp(-v_z^2/\sigma_v^2)$ where σ_v^2 is 0.65 and 0.45 km/s for $\theta = 0$ and 90°, respectively. The calculated $\beta(v)$ was obtained by substituting the calculated $I_\alpha(v_z)$ curves into Eq. (10).

(3) The width of the calculated curves for the cluster results does not change noticeably from weak cluster to strong cluster conditions.

Cluster-only TOF spectra are plotted in Fig. 2 and are fitted to Gaussian functions. A velocity-dependent anisotropy is calculated from the relation

$$\beta(v) = \frac{I_0(v_z) - I_{90}(v_z)}{\frac{1}{2}I_0(v_z) + I_{90}(v_z)}. \qquad (10)$$

Because $I_0(v_z)$ and $I_{90}(v_z)$ are well-described by Gaussian functions, $\beta(v_z)$ also has a Gaussian shape, both calculated and observed.

The c.m. translational energy distribution $P(E_{t,c.m.})$ for the monomer and cluster photodissociations were evaluated from the $I_0(v_z)$ and $I_{90}(v_z)$ and are plotted in Fig. 3. This determination requires knowing the mass of the counter fragment or, in other words, the parent cluster size. As noted above, the shape of the $I_\alpha(v_z)$ distributions attributable to clusters does not change as conditions for clustering are increased. If the first indication of clustering is assumed to be due to mostly dimers and some trimers, then it is reasonable to conclude that dimers and trimers dominant under increasing clustering conditions. Other evidence supporting this conclusion is previous work in our group using low-energy electron-impact ionization of $(CH_3I)_n$ in which we always observed a decreasing cluster size distribution, regardless of the intensity of our clustering conditions [20,28]. As it is not possible to ascertain the proportion of the $I_\alpha(v_z)$ that are due to dimers versus trimers, we evaluate $P(E_{t,c.m.})$ in Fig. 3 assuming one or the other cluster size in order to place boundaries on the actual translational energy distributions. The velocity-dependent anisotropy in Fig. 2 is clearly evident in Fig. 3. Interestingly, $P(E_{t,c.m.})$ is well described by a Maxwell–Boltzmann distribution despite the anisotropy. As summarized in Table 1, the translational energy release, though much less than for the monomer, is still sizable. Assuming

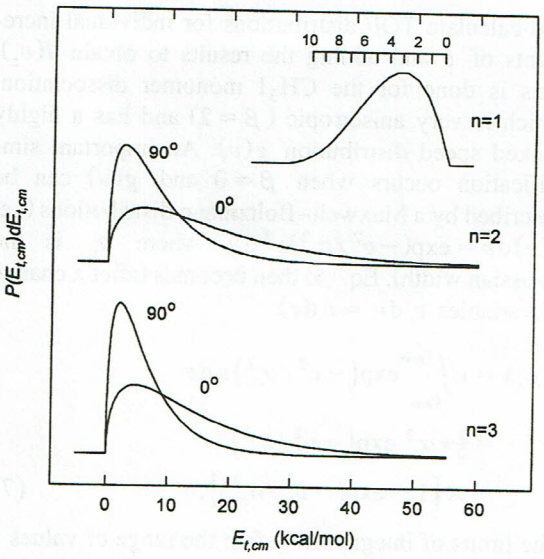

Fig. 3. The c.m. translational energy distribution for $(CH_3I)_n$ excitation at 266 nm and $I(^2P_{3/2})$ dissociation. Curves were obtained from the calculated $g(v_z)$ fits to $I_\alpha(v_z)$ in Fig. 2. The vibrational energies for the CH_3 ν_2 mode are shown for $n=1$. The $n=2$ and $n=3$ results represent how the calculated $P(E_{t,c.m.})$ are affected by assuming dissociation from dimer vs. trimer. Each curve is normalized to $\int P(E_{t,c.m.})\,dE_{t,c.m.} = 1$. The mean translational energies $\langle E_{t,c.m.} \rangle$ for $\theta = 0$ and 90°, respectively, are 17.1 and 8.1 kcal/mol assuming $n=2$, and 13.4 and 6.4 kcal/mol assuming $n=3$. $\langle E_{t,c.m.} \rangle$ for $n=1$ is 45.4 kcal/mol.

Table 1
Mean translational energy release for $I(^2P_{3/2})$ and spin–orbit branching ratios for $(CH_3I)_n$ photodissociation

Photolysis wavelength (nm)	n	Mean translational energy $< E_{t,c.m.} >$ (kcal/mol) [a]		Branching ratio $^2P_{3/2}/^2P_{1/2}$
		$\theta = 0°$	$\theta = 90°$	
266	1	45	–	0.37 [c]
	2,3	13–17	6–8	0.76
304	1	34	–	1.5
	2,3	21–27, 4–5 [b]	4–5	> 2.5

[a] Range of values depends on the assumption of $n=2$ versus $n=3$. See captions to Figs. 3 and 5.
[b] Two sets of energies represent bimodal distribution; the high-energy component is much less evident at $\theta = 90°$ than is the low-energy component.
[c] Refs. [31,32].

dimer conditions, the translational energies correspond to temperatures of 5700 and 2700 K for $\theta = 0$ and 90° fragment recoil, respectively.

The cluster results for 304 nm photolysis in Figs. 4 and 5 are similar to the 266 nm results with respect to the general appearance of the monomer and cluster TOF traces, aside from the lower recoil velocity for the longer wavelength. However, the 304 nm cluster results are markedly bimodal. The bimodal distribution is reasonably well fit by the sum of two Gaussian functions. (A closer inspection of the results for the 266 nm photolysis in Fig. 1c also shows that the data would be better fit by a sum of two Gaussian functions.) An additional velocity component that is peaked at high velocity and is anisotropic appears in Fig. 5b. This signal can be assigned to I_2 photodissociation on the basis of conservation of energy $E_t = h\nu - D_0 - E_{int}$ where $h\nu$ is the photon energy (4.08 eV), D_0 is the bond dissociation energy, which is 1.58 eV for I_2 (2.30 eV for CH_3I), and E_{int} is the internal energy of the counter fragment, which is 0 or 0.94 eV for I or I^*, respectively. The I atom signal due to I_2 has a higher order dependence on laser power than do the other I atom signals, which have the same dependence on laser power. This result is inconsistent with I atom coming from I_2 impurity, but rather from dissociation of I_2 that originated as a photoproduct from $(CH_3I)_n$ excitation. A similar signal was observed by Young for $(HI)_n$ clusters [16]. His careful laser power dependence measurements confirms the appearance of I^+ signal from the I_2 cluster photoproduct.

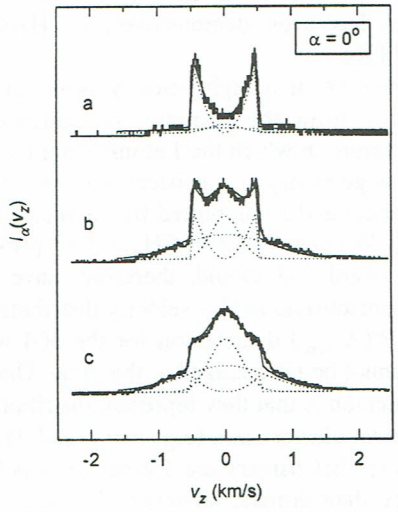

Fig. 4. $I_0(v_z)$ velocity spectra for $(CH_3I)_n$ excitation at 304 nm and $I(^2P_{3/2})$ detection as a function of increasing clustering conditions from (a) to (c). Calculated fits are shown (———) along with the individual contributions due to monomer and cluster excitation (· · ·). The cluster contribution was fitted by two Gaussian functions $\exp(-v_z^2/\sigma_v^2)$ of widths $\sigma_v^2 = 0.75$ and 0.35 km/s.

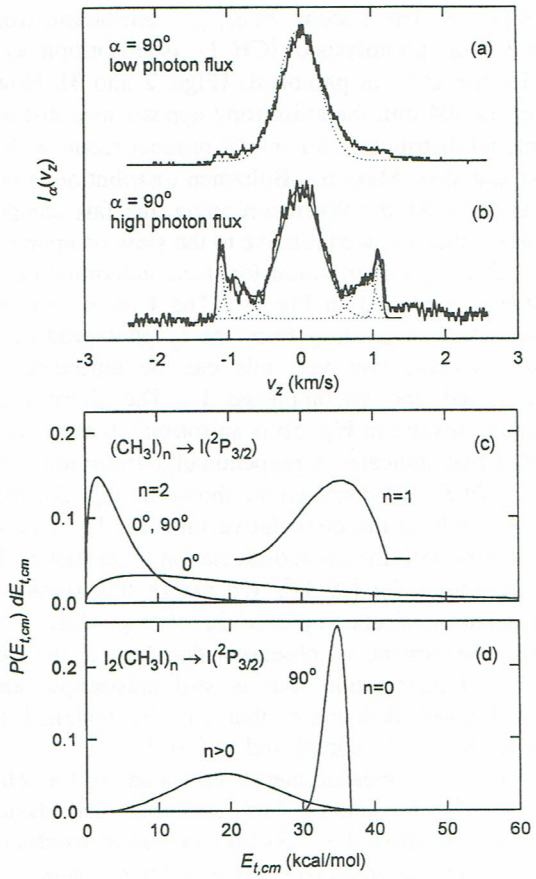

Fig. 5. (a),(b) $I_{90}(v_z)$ velocity spectra for $(CH_3I)_n$ excitation at 304 nm and $I(^2P_{3/2})$ detection as a function of photon flux. Calculated fits are shown (———) along with the individual contributions due to monomer and cluster excitation (· · ·). (c),(d) The c.m. translational energy distributions for CH_3I and I_2 precursors to detected I atom. Each curve is normalized to $\int P(E_{t,c.m.})\,dE_{t,c.m.} = 1$. The calculation in (c) for cluster dissociation assumes a value of $n = 2$. Values of $\langle E_{t,c.m.} \rangle$ are as follows: (c) ($n = 1$): 34.1; ($n = 2$): 21.5 and 4.6 kcal/mol for $\theta = 0$ and 0, 90°, respectively. (d) ($n = 0$): 33.9; ($n > 0$): 19.2 kcal/mol.

Translational energy distributions are plotted in Fig. 5c and Fig. 5d for $I(^3P_{3/2})$ photodissociated from CH_3I and I_2 as isolated molecules and in

complexes. The I atom $P(E_{t,c.m.})$ distribution from the 304 nm photolysis of $(CH_3I)_n$ is anisotropic as it is for the 266 nm photolysis (Figs. 2 and 3). However, at 304 nm, the anisotropy appears as a distinct bimodal distribution for $\theta = 0°$ product recoil with a fast and slow Maxwell–Boltzman distribution (Figs. 4 and 5c). At $\theta = 90°$ recoil angle, the fast component is much reduced relative to the slow component. The $P(E_{t,c.m.})$ distribution for these individual components is plotted in Fig. 5c. The I atom velocity distribution originating from the I_2 photoproduct is also bimodal, however, this can be attributed to complexed and uncomplexed I_2. The sharp high velocity feature in Fig. 5b is anisotropic with a value $\beta < 0$ that indicates a perpendicular transition, and has a $P(E_{t,c.m.})$ distribution, shown in Fig. 5d, that corresponds to the dissociative limit $I + I^*$. This is consistent with the photodissociation properties of I_2 in the ultraviolet [29,30]. We assign this signal to dissociation of uncomplexed I_2 photoproduct. Another component is observed that has a broader $P(E_{t,c.m.})$ distribution, but is still anisotropic and non-Maxwell–Boltzmann that can be assigned to dissociation of I_2 complexed to CH_3I.

Preliminary measurements were made of the relative yields of I and I* from monomer and cluster photodissociation. 2 + 1 REMPI excitation spectra of I atom were recorded over the wavelength range 303 to 305 nm, which encompasses three strong $^2P_{3/2}$ transitions and one $^2P_{1/2}$ transition. Pure monomer photofragment spectra were collected by detecting the entire TOF spectrum for $\theta = 0°$ recoil under non-clustering conditions (e.g. in Fig. 1a). Pure cluster photofragment spectra were recorded by detecting the TOF spectrum at $\theta = 90°$ recoil under clustering conditions (e.g. in Fig. 1c′). From the ratio of the I and I^* signals and the known branching ratio for monomer at 266 nm [31,32], it was possible to determine the branching ratios reported in Table 1. The significant observation is that the spin–orbit state distribution is greatly relaxed in cluster dissociation.

5. Discussion

We discuss four main results: (1) the anisotropy in the fragment velocity distribution, (2) the bimodal velocity distribution observed for 304 nm photolysis, (3) the measured I atom velocity distribution from I_2 photoproduct dissociation and (4) the relaxed spin–orbit distribution in cluster versus monomer photodissociation.

The anisotropy in the fragment velocity distribution can be understood as either a collisional relaxation or collisional scattering phenomena. Dissociated I atoms that have undergone few if any collisions in the complex will have an angle–velocity distribution approaching the highly peaked and anisotropic distribution observed for monomer photodissociation. As the residence time and number of collisions in the complex increase, the fragment will lose energy and anisotropy. In the limit of many collisions, one might expect a velocity distribution that is approximately Maxwell–Boltzmann, with the lowest energy fragments being completely isotropic. Loss of I atom anisotropy could be due to residence times in the cluster on the order of a rotational period, or due to angle-deflecting collisions. If the former property is significant, then the translational energy collisional relaxation rate may be determinable from E_t versus t plots, where t is obtained from β by relations for the rotational correlation function. The use of β as a rotational clock for molecules has been demonstrated by Hwang and El-Sayed [26].

The absence of a high velocity peak for I atom dissociating from the complex is evidence for a dimer structure in which the I atoms complex to each other. This geometry is consistent with the formation of I_2 product and is supported by geometry calculations [21]. We plan to detect CH_3, which presumably points outward and should, therefore, have a collisionless, anisotropic angle–velocity distribution. The bimodal $P(E_{t,c.m.})$ distribution for the 304 nm photolysis cannot be rationalized at this time. One possible explanation is that they represent distributions for two different cluster sizes (e.g. $n = 2$ and 3). It may be the case that trimers are formed in much lower abundance than dimers, however, the expected redshift of the trimer absorption relative to the dimer may enhance its excitation efficiency in the absorption wing at 304 nm. At the absorption peak at 266 nm, trimer excitation is not enhanced relative to dimer, possibly explaining the less evident bimodality at 266 nm. These results would be consistent with

a more energetic and anisotropic fragmentation for $n = 2$ and a more relaxed lower energy and isotropic fragment distribution for $n = 3$. A difficulty with this explanation, however, is the relative proportion of the two distributions does not change markedly with increasing clustering conditions. A second explanation is that the higher-energy $P(E_{t,c.m.})$ component is due to direct dissociation to $I(^2P_{3/2})$ and the low-energy distribution is due to dissociation to $I(^2P_{1/2})$ that undergoes a collisional relaxation to $^2P_{3/2}$. Collisional quenching of electronically excited states of atoms can be very efficient [33]. The difference in $\langle E_{t,c.m.} \rangle$ for these two components of about 15 kcal/mol is similar to the spin–orbit splitting of 21.6 kcal/mol. We plan to record a more complete set of data for upper spin–orbit state $I(^2P_{1/2})$ detection to reduce the possible explanations for this interesting effect.

The detection of I atom signal that can be positively assigned to dissociation of neutral I_2 photoproduct suggests a number of interesting properties of chemistry in $(CH_3I)_n$ clusters: (1) I_2 is formed in relatively high yield, even in small clusters of size $n = 2$ and 3. This property is also observed for $(HI)_n$ [16]. (2) The very sharp onset in the $I_2 \rightarrow I$ signal at $v_z = 1.2$ km/s in Fig. 5b is consistent with an I_2 energy (translational and rovibrational) that is much less than that for I atoms that escape the $(CH_3I)_n$ clusters. As noted earlier, Wang et al. measured a vibrational temperature of 1000 K for the I_2 product from $(CH_3I)_n$ photodissociation [21]; however, Fan et al. assert an upper limit of 300 K [22]. Both measurements are less than the Maxwell–Boltzmann translational temperatures for I atom of 2000–6000 K, as summarized in Table 1. For $(HI)_n$ photodissociation, Young reported I_2 TOF spectra that were unbroadened [16]. We plan a similar measurement for $(CH_3I)_n$ to determine the source of cooling of I_2. One obvious explanation is evaporation of CH_3I to leave bare I_2.

The significant increase in the $^2P_{3/2}$ to $^2P_{1/2}$ branching ratio for cluster versus monomer dissociation is intriguing because of the surface crossing in the A state that is responsible for the branching ratio in the monomer. It is tempting to ascribe the increased production of $^2P_{3/2}$ as being due to caging that allows the dissociation to proceed more adiabatically in the crossing region. Such a mechanism was invoked to explain an increased I/I^* branching ratio for CH_3I photodissociation on metal surfaces [34,35]. However, there are two other possible explanations. First, the $^2P_{1/2}$ state could be collisionally relaxed to $^2P_{3/2}$ as suggested above [33]. Second, the $^2P_{1/2}$ state carries less translational energy and so may have a lower probability of escaping the cluster than the $^2P_{3/2}$ state. Future experiments will measure the branching ratio as a function of I atom velocity (as opposed to total ion detection used here) to answer this question.

Acknowledgements

I thank Professor M.A. Young for valuable discussions and for providing a preprint of his article [16] prior to publication.

References

[1] C. Jouvet and B. Soep, Chem. Phys. Letters 96 (1983) 426.
[2] C. Jouvet, M. Boivineau, M.C. Duval and B. Soep, J. Phys. Chem. 91 (1987) 5416.
[3] C. Wittig, S. Sharpe and R.A. Beaudet, Accounts Chem. Res. 21 (1988) 341.
[4] S.K. Shin, Y. Chen, S. Nicholaisen, S.W. Sharpe, R.A. Beaudet and C. Wittig, Adv. Photochem. 16 (1991) 249, and references therein.
[5] S.I. Ionov, G.A. Bruker, C. Jaques, L. Valachovic and C. Wittig, J. Chem. Phys. 99 (1993) 6553.
[6] N.F. Scherer, L.R. Khundkar, R.B. Bernstein and A.H. Zewail, J. Chem. Phys. 87 (1987) 1451.
[7] N.F. Scherer, C. Sipes, R.B. Bernstein and A.H. Zewail, J. Chem. Phys. 92 (1990) 5239.
[8] T. Baumert, S. Pedersen and A.H. Zewail, J. Phys. Chem. 97 (1993) 12447.
[9] J.S. Riley and T. Baer, Intern. J. Mass Spectrom. Ion Processes 131 (1994) 295.
[10] K. Ohashi and N. Nishi, J. Chem. Phys. 98 (1993) 390.
[11] C.M. Roehl, J.T. Snodgrass, C.A. Deakyne and M.T. Bowers, J. Chem. Phys. 94 (1991) 6546, and references therein.
[12] R. Ogorzalek Loo, G.E. Hall, H.-P. Haerri and P.L. Houston, J. Phys. Chem. 92 (1988) 5.
[13] S.M. Penn, C.C. Hayden, K.J. Carlson Muyskens and F.F. Crim, J. Chem. Phys. 89 (1988) 2909.
[14] J. Segall, Y. Wen, R. Singer, C. Wittig, A. Garcia-Vela and R.B. Gerber, Chem. Phys. Letters 207 (1993) 504.
[15] R.J. Bemish, E.J. Bohac, M. Wu and R.E. Miller, J. Chem. Phys. 101 (1994) 9457.
[16] M.A. Young, J. Chem. Phys., in press.

[17] D.M. Willberg, M. Gutmann, J.J. Breen and A.H. Zewail, J. Chem. Phys. 96 (1992) 198.
[18] J.M. Papanikolas, V. Vorsa, M.E. Nadal, P.J. Campagnola, H.K. Buchenau and W.C. Lineberger, J. Chem. Phys. 99 (1993) 8733.
[19] S.P. Sapers, V. Vaida and R. Naaman, J. Chem. Phys. 88 (1988) 3638.
[20] J.A. Syage and J. Steadman, Chem. Phys. Letters 166 (1990) 159.
[21] P.G. Wang, Y.P. Zhang, C.J. Ruggles and L.D. Ziegler, J. Chem. Phys. 92 (1990) 2806.
[22] Y. Fan, K.L. Randall and D.J. Donaldson, J. Chem. Phys. 98 (1993) 4700.
[23] R.A. Hertz and J.A. Syage, J. Chem. Phys. 100 (1994) 9265.
[24] J.A. Syage, J. Chem. Phys., in press.
[25] R. Ogorzalek Loo, H.-P. Haerri, G.E. Hall and P.L. Houston, J. Chem. Phys. 90 (1989) 4222.
[26] H.J. Hwang and M.A. El-Sayed, J. Chem. Phys. 94 (1991) 4877.
[27] T.A. Spiglanin and D.W. Chandler, Chem. Phys. Letters 141 (1987) 428.
[28] J.A. Syage, J. Chem. Phys. 92 (1990) 1804.
[29] R.D. Clear and K.R. Wilson, J. Mol. Spectry. 47 (1973) 39.
[30] H.J. Hwang and M.A. El-Sayed, J. Phys. Chem. 95 (1991) 8044.
[31] S.J. Riley and K.R. Wilson, Faraday Discussions Chem. Soc. 53 (1972) 132.
[32] W.P. Hess, S.J. Kohler, H.K. Haugen and S.R. Leone, J. Chem. Phys. 84 (1986) 2143.
[33] I.V. Hertel, Advan. Chem. Phys. 45 (1981) 341.
[34] E.T. Jensen and J.C. Polanyi, J. Phys. Chem. 97 (1993) 2257.
[35] D.H. Fairbrother, K.A. Briggman, P.C. Stair and E. Weitz, J. Chem. Phys. 102 (1995) 7267.